Journal of Alloys and Compounds 509 (2011) 1768–1773

Contents lists available at ScienceDirect

Journal of Alloys and Compounds

journal homepage: www.elsevier.com/locate/jallcom

Effects of Mg substitution on the structural, optical, and electrical properties of $CuAlO_2$ thin films

H.F. Jiang[a,b], X.B. Zhu[a,*], H.C. Lei[a], G. Li[a], Z.R. Yang[a], W.H. Song[a], J.M. Dai[a], Y.P. Sun[a], Y.K. Fu[c]

[a] Key Laboratory of Material Physics, Institute of Solid State Physics, Chinese Academy of Sciences, Hefei 230031, China
[b] Department of Physics, Chizhou College, Chizhou 24700, China
[c] Shandong University of Science and Technology, Qingdao 266510, China

ARTICLE INFO

Article history:
Received 6 June 2010
Received in revised form 8 October 2010
Accepted 10 October 2010
Available online 21 October 2010

Keywords:
$CuAlO_2$
Delafossite
Optical property
Electrical property
Chemical solution deposition

ABSTRACT

Mg-doped $CuAlO_2$ thin films are prepared by the chemical solution method. The XRD results show that the solid solubility of Mg species on Al sites in $CuAlO_2$ lattice is lower than 2 at.%. When less than 2 at.% of Mg is added to the $CuAlO_2$ film, the surface roughness of the films was reduced with Mg substitution. Moreover, the *c*-axis orientation of the films improves because the in-plane fusion between $CuAlO_2$ crystallites is hindered. Optical and electrical measurements show that substituting Al^{3+} in the films with Mg^{2+} increases both their transmittance in the visible region and their optical band gaps. As well, their electrical conductivity is enhanced. At 300 K, the conductivity of the 1 at.% Mg-doped sample is up to 5.2×10^{-3} S/cm. Thus, Mg-doped $CuAlO_2$ films may have potential applications as transparent conductive oxides.

Published by Elsevier B.V.

1. Introduction

Transparent conducting oxides (TCOs) have attracted much attention because of their functional combination of transparency and electrical conductivity. In general, most of the known TCOs are n-type materials. N-type materials, such as tin oxide, zinc oxide, indium oxide, and cadmium oxide, were popularly used in optoelectronics before 1997 [1–4]. For the use in transparent electronics technology, a p–n junction is required. Therefore, p-type TCO is highly sought after. p-Type $CuAlO_2$ thin films were first fabricated in 1997 [5]. Since then, many attempts have been made to grow $CuAlO_2$ thin films with high performance (high conductivity and high transparency). Various production methods, such as pulsed laser deposition (PLD) [6], RF magnetron sputtering [7], chemical vapor deposition [8,9], spray pyrolysis [10,11], and sol-gel processes [12–14], among others, have been reported. Unfortunately, some difficulties, including high crystallization temperatures, secondary phase introductions, low transmittance, and low conductivity were encountered with these techniques. These problems have limited the applications of $CuAlO_2$ thin films in photovoltaic cells, gas sensors, light-emitting diodes, transistors, and so on.

$CuAlO_2$ has an ABO_2 delafossite structure (A = Cu, Ag, Pd, Pt; B = Sc, Cr, Fe, Y, La, Al, Ni, Rh, Co). In this structure, monovalent cation A is coordinated with two oxygen atoms along the *c*-axis, forming an O–Cu–O dumbbell structure. Trivalent cation B is coordinated with six oxygen atoms, forming an edge-sharing BO_6 octahedron. The Cu^+ layers and $B^{3+}O_2$ layers alternately stack along the *c*-axis. Recent studies presented the O–Cu–O dumbbell layers are important for hole transport and oxygen intercalation [15,16]. As such, the substitution of bivalent cations in B sites, such as that in $CuSc_{1-x}Mg_xO_2$ [17], $CuCr_{1-x}Mg_xO_2$ [18], $CuRh_{1-x}Mg_xO_2$ [19], $CuY_{1-x}Ca_xO_2$ [20], $CuIn_{1-x}Ca_xO_2$ [21], and $CuFe_{1-x}Ni_xO_2$ [22], is generally considered a direct and effective route to increasing p-type electrical conductivity because this substitution can induce the change of Cu valence state from +1 to +2 in the O–Cu–O dumbbell layers according to the valence equilibrium in defect chemistry and then realize the hole hopping from the Cu^{2+} to Cu^+. It can be expressed as $Cu^+ + Al^{3+} \rightarrow Cu^+ + Mg_{Al}^{2+} + h \rightarrow Cu^{2+} + Mg_{Al}^{2+}$, where Mg_{Al}^{2+} and h denote the Mg^{2+} cation on the Al^{3+} site and a positive hole, respectively. To date, a large number of experiments have been devoted to research on the effects of Mg substitution in isostructure $CuCrO_2$ semiconductors. For example, Sadik et al. reported the electrical transport of $CuCr_{1-x}Mg_xO_2$ thin films grown by pulsed laser deposition, and found that the optimal atomic ratio of Mg to Cr was 3 at.% [23]. Nagarajan et al. investigated the p-type conductivity of Mg-doped $CuCrO_2$ oxide thin films deposited using RF sputtering; they found that the optimal value for doping was 5 at.% [24]. Through solid state reactions, Maignan et al.

* Corresponding author. Tel.: +86 551 5592757; fax: +86 551 5591434.
E-mail address: xbzhu@issp.ac.cn (X.B. Zhu).

0925-8388/$ – see front matter. Published by Elsevier B.V.
doi:10.1016/j.jallcom.2010.10.036

found that the solubility of Mg^{2+} in $CuCrO_2$ compounds was not over 1 at.% [25]. These studies show that the doping of the same cation in $CuCrO_2$ materials could be influenced by the preparation methods of the material.

To the best of our knowledge, only Dong et al. [26] reported on Mg substitution in $CuAlO_2$ thin films deposited using the RF magnetron sputtering technique. In their experiments, polycrystalline targets of $CuAl_{1-x}Mg_xO_2$ ($x = 0$, 0.01, 0.02 and 0.05) used for sputtering were synthesized by heating a stoichiometric mixture of Cu_2O (99%), $Al(OH)_3$ (99.9%) and MgO (99.9%) at 1373 K for 10 h. They found that the solubility of Mg species in the $CuAlO_2$ lattice is up to 5 at.%, and the crystalline quality of the films declines with increasing Mg concentration. In this paper, we report the preparation of $CuAl_{1-x}Mg_xO_2$ thin films by the chemical solution deposition (CSD) method, and investigate the effects of Mg substitution on the structural, optical and electrical properties of the $CuAlO_2$ thin films produced.

2. Experimental

Four solutions of $CuAl_{1-x}Mg_xO_2$ ($x = 0$, 0.005, 0.01 and 0.02) used for spin-coating were prepared by dissolving mixtures of $Cu(CH_3COO)_2{\cdot}H_2O$ (99%), $Al(NO_3)_3{\cdot}9H_2O$ (99%), and $Mg(NO_3)_2{\cdot}6H_2O$ (99%) in $CH_3CH(OH)CH_3$ (99.7%). The molar ratio of Mg to Cu in each solution was determined by the x value and then the molar ratio of Al species was equal to the $(1 - x)$ value. The mixtures were stirred for 4 h in order to obtain well-mixed solutions. The concentrations of these homogenous solutions were 0.2 M.

Before deposition, sapphire substrates were cleaned sequentially with acetone, ethanol, and deionized water in an ultrasonic cleaner. Droplets of these solutions were spin-coated onto (0 0 1) sapphire substrates at a speed of 6000 rpm for 20 s. The deposited films were preheated for 20 min at 400 °C in a quartz tube furnace to evaporate the solvent and remove organic residues. To obtain the desired thickness, spin-coating and preheating were repeated six times. Finally, the deposited films were annealed for 6 h at 900 °C under ultra-pure nitrogen gas at a flow rate of 150 mL/min. According to Ref. [27], $CuAlO_2$ is not thermodynamically stable at 900 °C in air. Thus, nitrogen or argon must be used as an annealing gas to obtain the pure delafossite phase. After annealing, the furnace was allowed to cool down naturally to room temperature. In this paper, the thickness of all the obtained films was about 200 nm (Fig. 4).

Film crystallinity was examined using a grazing incidence X-ray diffractometer (GIXRD, Philips designed X'Pert Pro type) (grazing angle $\alpha = 1°$). Field emission-scanning electron microscope (FE-SEM) was used to determine surface patterns. Optical transmittance was recorded using a UV–vis-NIR spectrophotometer (CARY-5E) at a fixed incidence angle perpendicular to the film surface and within the range of 200–800 nm. Uncoated substrate was used as a reference for transmittance measurements. In the inset of Fig. 7, the preparation of the $CuAl_{1-x}Cr_xO_2$ thin films followed the above mentioned CSD route for comparison. DC resistivity was measured using the four-probe configuration. Silver paste was used to create good ohmic contacts. Hall measurements were carried out at room temperature using the van der Pauw method.

3. Results and discussion

Fig. 1 shows the GIXRD patterns for the synthesized $CuAl_{1-x}Mg_xO_2$ ($x = 0$–2%) samples. For the sake of description, we define here the $CuAl_{1-x}Mg_xO_2$ films with $x = 0\%$, 0.5%, 1% and 2% as the sample Mg_0, $Mg_{0.5}$, Mg_1 and Mg_2, respectively. When the amount of Mg substitution is below 2 at.%, the obtained films are phase-pure and the structure can be indexed to delafossite with a space group of R-3m. This result for solid solubility differs from the result reported by Dong et al. [26]. However, the Mg^{2+} ionic radius (0.66 Å) is almost equal to that of the Cr^{3+} radius (0.63 Å), and the Mg content in $CuCr_{1-x}Mg_xO_2$ thin films derived from various preparation methods are not over 5 at.% under the premise of a single delafossite phase. Furthermore, the CSD method is a novel route used to obtain thin films with compositional homogeneity. Further work is necessary to clarify such inconsistencies between studies.

Each peak in Fig. 1 is indexed according to standard powder data (JCPDS, No. 35-1401). When $x = 2\%$, the diffraction peaks corresponding to the delafossite structure are strongly suppressed,

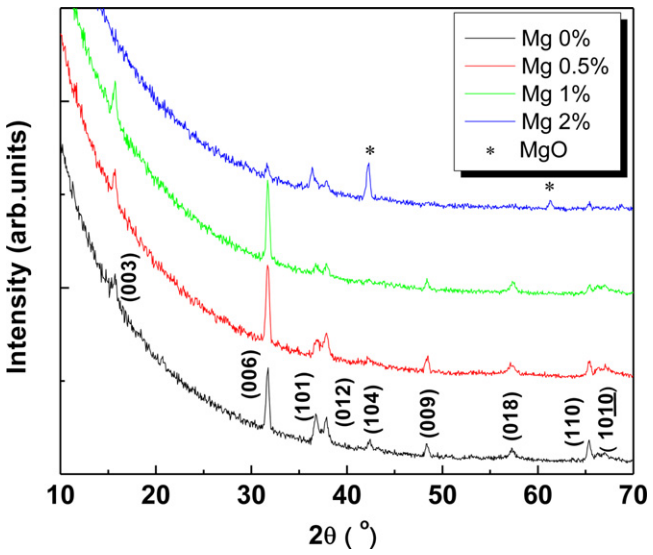

Fig. 1. GIXRD patterns for the $CuAl_{1-x}Mg_xO_2$ ($0 \le x \le 0.02$) thin films. The asterisks denote the impurity phase MgO.

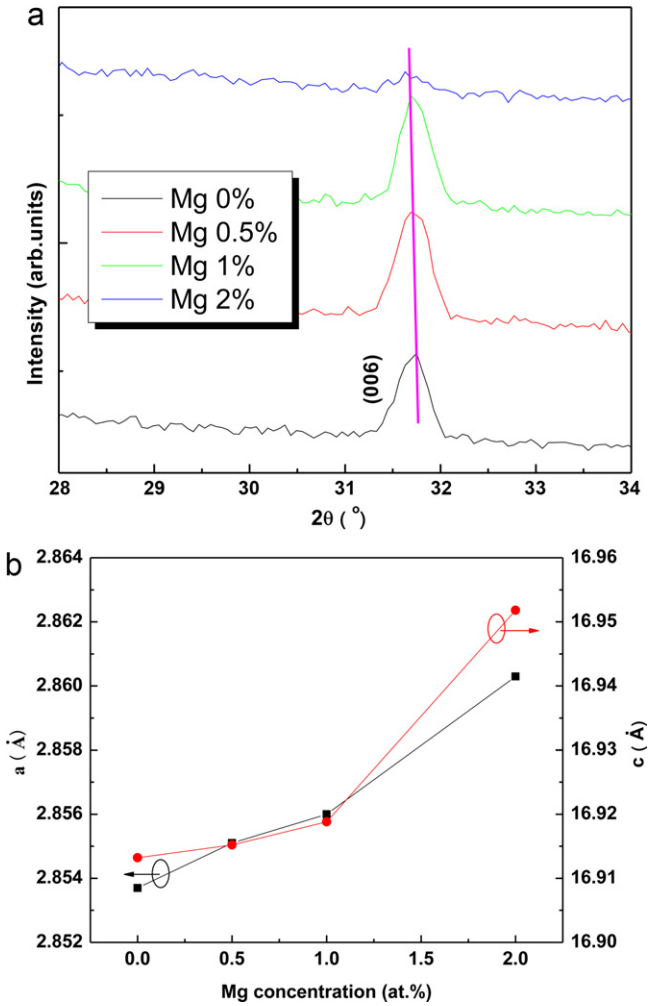

Fig. 2. (a) Magnified XRD patterns of the (0 0 6) peaks of the $CuAl_{1-x}Mg_xO_2$ thin films. The oblique solid line reflects the shift of (0 0 6) peaks. (b) Variation of calculated lattice parameters a and c with Mg concentration according to the formula $2d \sin\theta = n\lambda$ and the positions of (0 0 6) and (0 1 2) peaks.

while a peak at 42.3° is strengthened and another peak at 61.3° appears. The peak at 42.3° is not believed to be a sign of (0 1 4) preferred orientation growth. Instead, a new phase of MgO is thought to have been produced, especially when the peak at 61.3° is taken into account.

With increasing x, the *c*-axis orientation of the samples Mg_0, $Mg_{0.5}$ and Mg_1 increases sequentially. This result also differs from that found by Dong et al. [26]. Here, a possible interpretation of the variation of the *c*-axis orientation is presented. The primary characteristic of the chemical solution deposition process is that $CuAlO_2$ crystal nuclei form dispersively, accompanying both the decomposition and evaporation of chemical organics. These crystal nuclei on the Al_2O_3 (0 0 1) substrate were all expected to be of *c*-axis orientation because of the match of both the crystal symmetry (rhombohedral crystal system) and the lattice parameter (the O–O distances for $CuAlO_2$ and (0 0 1) Al_2O_3 are 2.86 and 2.70 Å, respectively) between the $CuAlO_2$ crystallite and the Al_2O_3 (0 0 1) substrate. However, during annealing, these crystal nuclei grew up and fused with each other in the in-plane direction, resulting in *c*-axis degeneration. This is why thicker films have worse *c*-axis orientation. Mg introduction causes difficulties in the in-plane fusion between crystallites. Thus, the growth of the crystallites tends to become out-of-plane (*c*-axis). With increasing Mg content, the enhancement of *c*-axis orientation appears. As a layered semiconductor possessing anisotropic conductivity [28], the texture growth of the three films favors increases in p-type electrical conductivity.

The Mg^{2+} ionic radius is 0.66 Å while that for Al^{3+} is 0.51 Å. Due to the mismatch between the ionic radii, the substitution of Mg^{2+} ions in Al^{3+} sites induces lattice distortion. This is clearly seen in the magnified XRD patterns of the (0 0 6) peak, displayed in Fig. 2(a). An oblique solid line, which reflects the shift of the (0 0 6) peaks, is also shown. The shift to lower angles occurs with increasing x. This finding is highly consistent with the variation of lattice parameters shown in Fig. 2(b). Using the Scherrer formula ($D = 0.9\lambda/(\beta\cos\theta)$) and the FWHM of the (0 0 6) peak, the crystallite sizes for the samples Mg_0, $Mg_{0.5}$ and Mg_1 are calculated to be 29.4, 30.1, and 33.8 nm, respectively.

Fig. 3 shows the morphology of the obtained $CuAl_{1-x}Mg_xO_2$ thin films. A needle-like surface forms for the undoped Mg_0 film. Judging from the colors of the grains, the film seems to consist of several phases. However, the XRD patterns indicate that the film is composed of pure delafossite phases. Therefore, the difference in the colors could be due to the high surface roughness present in the sample. When the amount of Mg is increased to 0.5 at.%, the surface morphology of the $Mg_{0.5}$ film significantly improves. Compared to the undoped film, $Mg_{0.5}$ has a much smoother surface except for some holes. When the Mg content is further increased to 1 at.%, the Mg_1 film becomes smoothest and most compact. The morphological evolution of the three films ($x < 2$ at.%) illustrates the improvement of surface roughness by Mg substitution. When *x* is equal to 2 at.%, bigger grains are extruded on the surface of the film, causing an inhomogeneous morphology. Initially, it was assumed that larger grains were associated with MgO impurity phases, and this hypothesis was expected to be verified by energy dispersive spectral measurements. However, due to issues regarding the thickness of the films (~200 nm) and the penetration depth of the X-ray used (much higher than 200 nm), the obtained results (not shown here) were undesirable. Thus, the origin of the larger grains remains unclear.

Fig. 5 illustrates the transmittance of $CuAl_{1-x}Mg_xO_2$ thin films in the range of 200–800 nm. The transmittance of the samples Mg_0, $Mg_{0.5}$, Mg_1 and Mg_2 at 500 nm are 71.1%, 74.9%, 74.8%, and 48.7%, respectively. Such high values for the three films ($x < 2$ at.%) produced by the CSD method are comparable to those obtained by physical methods, such as PLD and RF sputtering. In the vis-

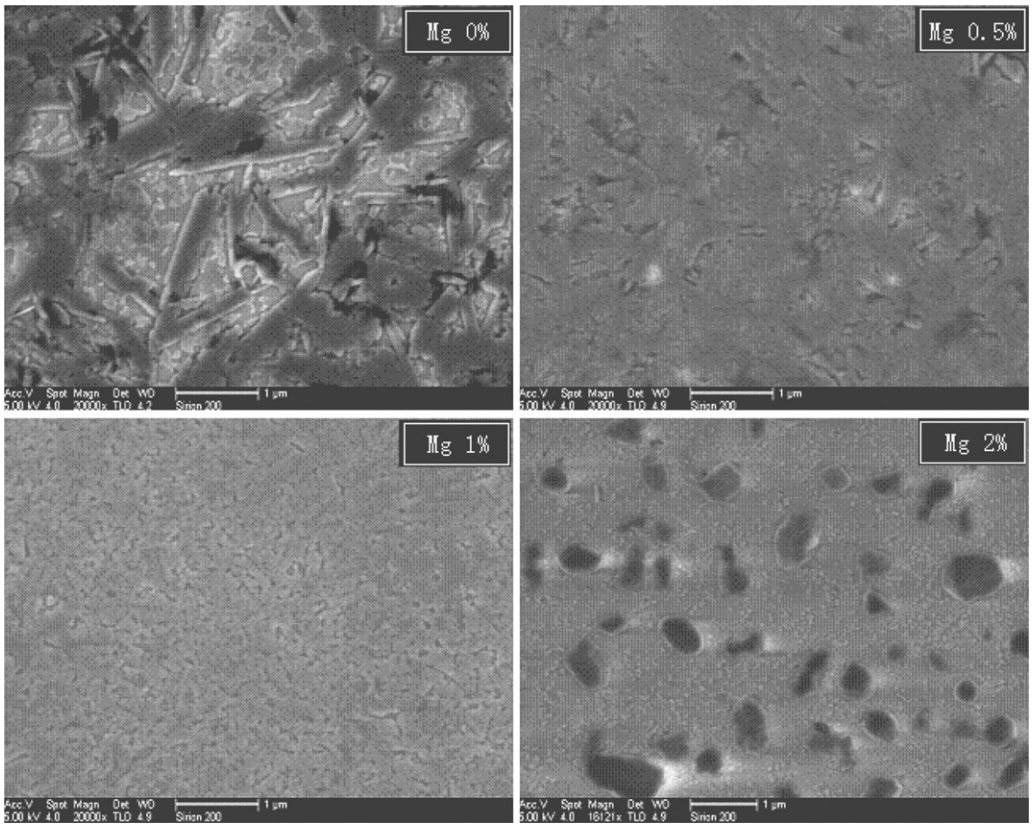

Fig. 3. SEM images of the surface morphology of the $CuAl_{1-x}Mg_xO_2$ thin films.

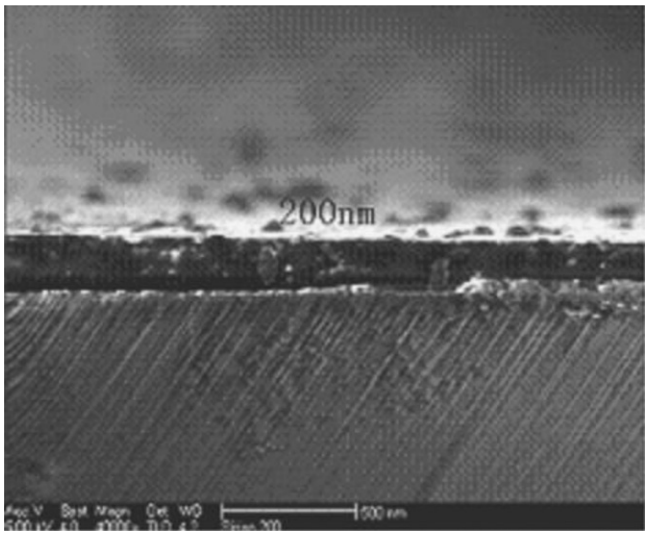

Fig. 4. Cross-sectional SEM image of the thickness of the $CuAl_{1-x}Mg_xO_2$ thin films.

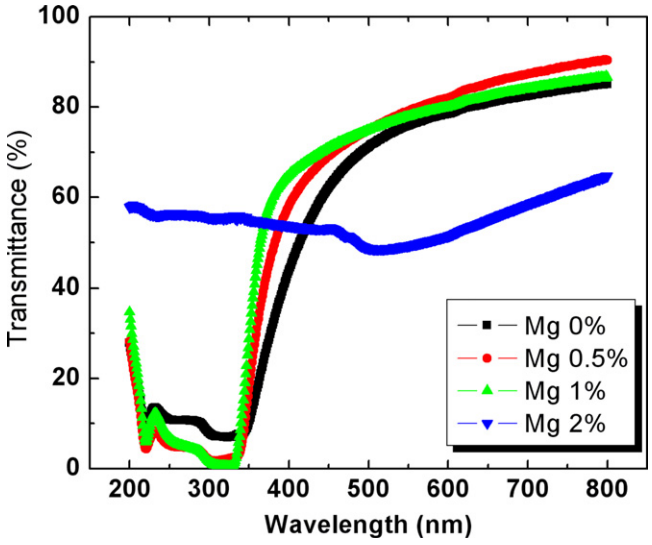

Fig. 5. Transmittance of the $CuAl_{1-x}Mg_xO_2$ thin films as a function of wavelength ranging from 200 to 800 nm.

ible region, the transmittance of the Mg-doped films is a little higher than that of the undoped film. Given the surface morphology of these films, the improvement in their optical transparency could be due to decreased surface scattering (Fig. 3). Between 350 and450 nm, the plots of the films, except for the sample Mg_2, become steeper with increasing x. This reflects improvements in the crystallinity of the samples with increasing Mg substitution [29], which is highly consistent with the XRD results in Fig. 1.

Tauc's relation, expressed as $(\alpha h\gamma)^2 = A(h\gamma - E_g)$ [30], was used to calculate the optical band gaps of the $CuAl_{1-x}Mg_xO_2$ thin films. The intersection point of each linear fit to $h\gamma$-coordinate corresponds to the optical band gap of each sample. In Fig. 6, the band gaps of the samples Mg_0, $Mg_{0.5}$ and Mg_1 are 3.32, 3.51, and 3.58 eV, respectively. The change in optical band gaps could not be interpreted using Burstein-Moss shift or quantum size effect according to the above calculations for crystallite sizes [31]. The optical anomaly in 13 group delafossites of $Cu^{1+}M^{3+}O_2$, such as $CuAlO_2$, $CuGaO_2$, and $CuInO_2$, has remained debatable [32]. If the simple consideration that direct optical band gaps increase with increasing M^{3+} ionic radius, i.e., $gap_{CuAlO_2} < gap_{CuGaO_2} < gap_{CuInO_2}$, is assumed, then the increase in the optical band gaps of the

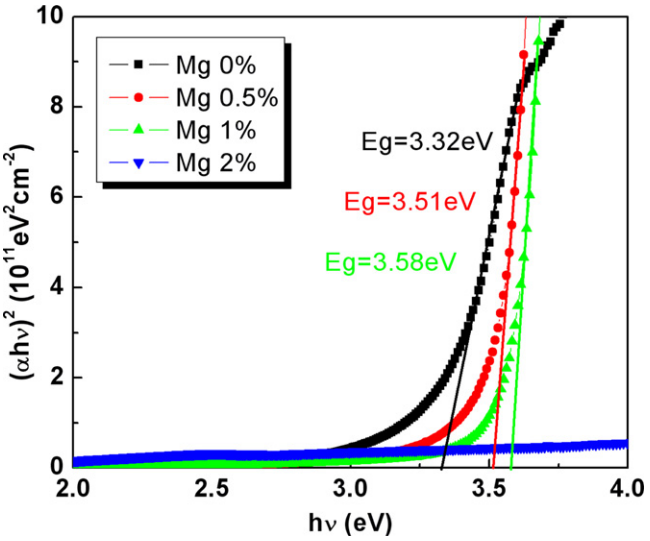

Fig. 6. Optical band gaps of the $CuAl_{1-x}Mg_xO_2$ thin films calculated by using Tauc's relation.

$CuAl_{1-x}Mg_xO_2$ thin films could be simply attributed to Mg substitution as an effect of increasing M^{3+} ionic radius. The sample Mg_2 does not have an optical band gap, suggesting that this film loses the function of optical window which means selective transmission for incident light.

The optical transmittance of the films in the ultraviolet region (175–325 nm) provides information regarding the structure of the valence band maximum (VBM). Studies involving this region have not yet been reported in relevant publications. Enlarged plots of this region are shown in Fig. 7. The undoped sample Mg_0 has higher optical transmittance, while the transmittance of the sample $Mg_{0.5}$ is lowered integrally on the premise of keeping the curve unchanged. This implies the increase of electron occupation in the VBM. However, the curve of the sample Mg_1 differs significantly from the two other samples (Mg_0 and $Mg_{0.5}$). The experimental results are entirely different from the results obtained for Cr-doped $CuAlO_2$ thin films investigated earlier by our group. In such films, transmittance in the ultraviolet region presented monotonous decreases with Cr doping (shown in the inset of Fig. 7). Consid-

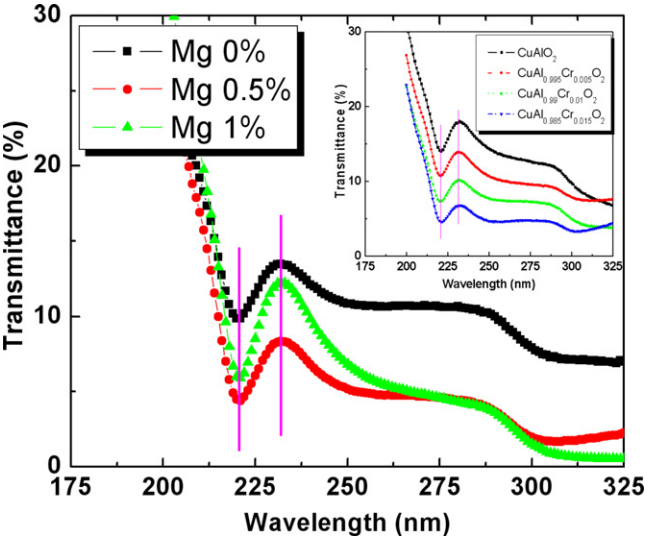

Fig. 7. Enlarged plots of the transmittance of the $CuAl_{1-x}Mg_xO_2$ thin films in the ultraviolet region. The inset shows the transmittance of the $CuAl_{1-x}Cr_xO_2$ ($0 \le x \le 0.015$) thin films in the same region for comparison.

ering the contribution of Cr 3d states to the VBM [33], enhanced hybridization is expected. In the present films, however, because Mg^{2+} ions have no d electrons, new considerations are proposed here. First, Mg substitution leads to bigger M^{3+} ionic radii, which in turn increases the cell parameter *a*. Increasing this parameter simultaneously induces the increase of O interstitials in triangular Cu layers [34], and the decrease of overlapping between Cu 3d states in the *ab* planes. On one hand, the increase of O interstitials may cause hybridization strengthening because the VBM is composed of hybridized Cu 3d and O 2p anti-bonding states [32], which can cause increases in the total density of states. On the other hand, the character of the VBM is mainly dominated by overlapping between Cu 3d states when *x* is greater than 0.5% because the off-stoichiometric oxygen is limited [35].

Fig. 8 shows the resistivity of the films as a profile of temperature in the range of 200–310 K. From the plots, the three samples all exhibit semiconductor-like electrical behavior ($d\rho/dT < 0$). As known, $CuAlO_2$ is a layered p-type semiconductor and Al ions in its structure are in the trivalent state. Bivalent cations, such as Mg^{2+}, Ca^{2+}, and Zn^{2+}, doped onto Al^{3+} sites can increase p-type conductivity mainly by contributing to the hole concentration [26,36,37]. This conclusion has been thoroughly verified by many experiments involving the delafossite structure. Enlarged plots of the films in the temperature range of 280–310 K are shown in the inset of Fig. 8. At 300 K, the resistivity of the films with $x = 0\%$, 0.5%, and 1% are 822, 342, and 193 Ω·cm, respectively. These values are slightly larger than those of films with the same composition but prepared by the PLD method, indicating that CSD technique needs to be further improved.

From the analysis of the transmittance in the ultraviolet region, it appears that both Mg^{2+} cations and O interstitials contribute to hole carriers. In addition to the carrier concentration, mobility is another important factor that influences conductivity ($\sigma = en\mu$). From the XRD and SEM results, with increasing Mg substitution, both the enhancement of the *c*-axis orientation and improvements of morphology are expected to increase the mobility of holes. In order to confirm this deduction, Hall measurements were carried out on the three films at room temperature using the van der Pauw method. The positive Hall coefficient measured for these films verifies the p-type conductivity of the samples. The carrier concentrations are 2.29×10^{16}, 4.82×10^{16}, and $7.58 \times 10^{16}\ cm^{-3}$ for the samples Mg_0, $Mg_{0.5}$ and Mg_1, respectively. From these data,

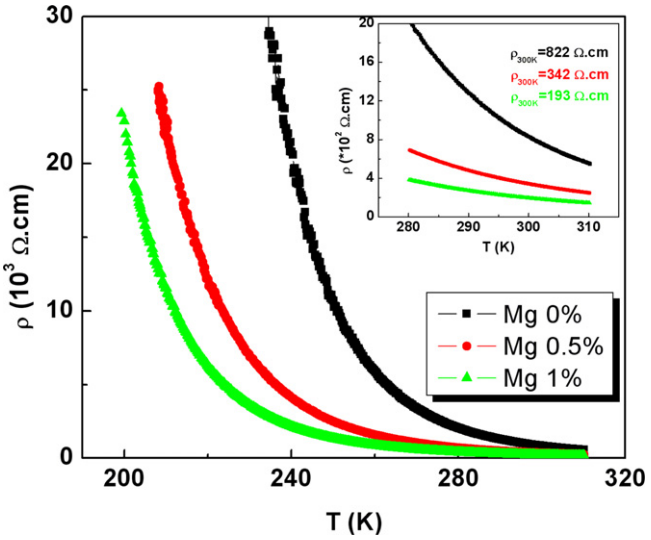

Fig. 8. Temperature dependence of the resistivity of the $CuAl_{1-x}Mg_xO_2$ thin films. The inset shows the resistivity of these samples in the temperature range from 280 to 310 K.

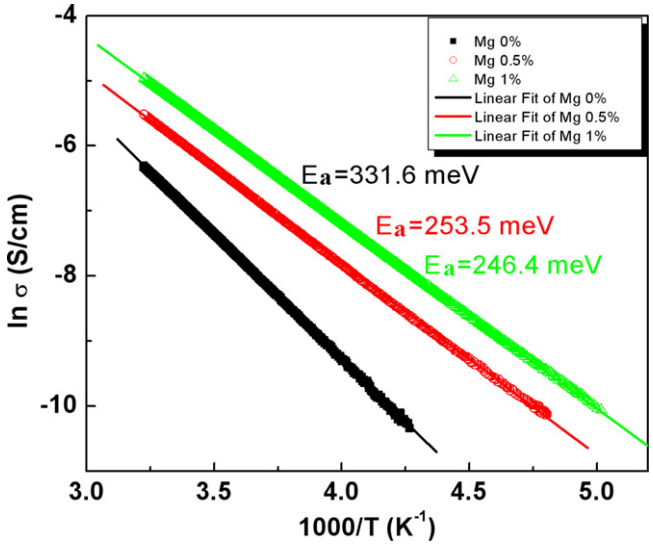

Fig. 9. Plots of $\ln\sigma$ vs. $1000/T$ of the $CuAl_{1-x}Mg_xO_2$ thin films ($x = 0$, 0.5%, 1%). The linear fit of each curve determines the activation energy E_a of each sample.

the calculated mobility for Mg_0, $Mg_{0.5}$ and Mg_1 are 3.31×10^{-1}, 3.79×10^{-1}, and $4.27 \times 10^{-1}\ cm^2\ V^{-1}\ s^{-1}$, respectively. These values show that the increase in conductivity is a result of the increase of both the carrier concentration and mobility.

The plots of $\ln\sigma$ vs. $10^3/T$ are presented in Fig. 9 to better understand the conduction mechanism of the films. From the figure, the data obtained can fit the thermal activation model well, similar to the results reported by Tate et al. [38]. The activation energy is the energetic difference from an acceptor level to the valence band maximum (VBM) for p-type semiconductors, or from the conduction band minimum (CBM) to a donor level for n-type semiconductors. The activation energies are 331.6, 253.5, and 246.4 meV for the samples Mg_0, $Mg_{0.5}$ and Mg_1, respectively, indicating that Mg-doping changes the position of the acceptor level in the band gap. The variation trend is the same as that for resistivity, confirming once again the helpful effect of Mg substitution on the electrical properties of the films.

4. Conclusion

We successfully prepared $CuAl_{1-x}Mg_xO_2$ thin films on sapphire substrates by the CSD method. XRD and SEM results reveal that the thin films crystallize in 3R-delafossite structure when *x* is lower than 2 at.%, and that Mg substitution on Al sites improves the morphology of the films produced. The optical band gaps increase sequentially with increasing *x* ($0 \le x \le 1\%$), due possibly to the size effect of the M^{3+} ion in delafossite $Cu^{1+}M^{3+}O_2$. Changes in transmittance in the ultraviolet region indicate changes in both the degree of hybridization and electron occupation in the VBM. Resistivity measurements show that Mg doping is helpful in increasing p-type conductivity. $CuAl_{1-x}Mg_xO_2$ thin films synthesized by the CSD method have higher optical transparency, comparable even to films prepared by other physical methods despite their lower electrical conductivity. These results suggest that the CSD method is a novel and valuable route for the preparation of oxide films.

Acknowledgements

This work was supported by the National Key Basic Research, under Contract No. 2007CB925002, and the National Nature Science Foundation of China, under Contract Nos. 10774146 and 50802096. Grants were also provided by the Anhui Province NSF

(No. 070414162) and Director's Fund of Hefei Institutes of Physical Science, Chinese Academy of Sciences.

References

[1] R.K. Gupta, K. Ghosh, R. Patel, P.K. Kahol, Applied Surface Science 255 (2009) 6252.
[2] F. Yakuphanoglu, Journal of Alloys and Compounds 470 (2009) 55.
[3] H.F. Liu, G.X. Hu, H. Gong, Journal of Crystal Growth 311 (2009) 268.
[4] M. Sahal, B. Hartiti, A. Ridah, M. Mollar, B. Mar, Microelectronics Journal 39 (2008) 1425.
[5] H. Kawazoe, M. Yasukawa, H. Hyodo, M. Kurita, H. Yanagi, H. Hosono, Nature 389 (1997) 939.
[6] M.N. Spallart, S.P. Pai, R. Pinto, Thin Solid Films 515 (2007) 8641.
[7] W. Lan, M. Zhang, G.B. Dong, P.M. Dong, Y.Y. Wang, H. Yan, Materials Science and Engineering B 139 (2007) 155.
[8] J.L. Cai, H. Gong, Journal of Applied Physics 3 (2005) 033707.
[9] Z. Lockman, L.P. Lin, C.K. Yew, S.D. Hutagalung, Solar Energy Materials and Solar Cells 93 (2009) 1383.
[10] C. Bouzidi, H. Bouzouita, A. Timoumi, B. Rezig, Materials Science and Engineering B 118 (2005) 259.
[11] A. Belafhaili, M.A. Aouaj, R. Diaz, A. Belayachi, F. Rueda, M. Abd-Lefdil, Sensor Letters 5 (2009) 672.
[12] K. Tonookaa, K. Shimokawa, O. Nishimura, Thin Solid Films 411 (2002) 129.
[13] S. Gotzendorfer, C. Polenzky, S. Ulrich, P. Lobmann, Thin Solid Films 518 (2009) 1153.
[14] H.F. Jiang, H.C. Lei, X.B. Zhu, G. Li, Z.R. Yang, W.H. Song, J.M. Dai, Y.P. Sun, Y.K. Fu, Journal of Alloys and Compounds 487 (2009) 404.
[15] D.O. Scanlon, K.G. Godinho, B.J. Morgan, G.W. Watson, The Journal of Chemical Physics 132 (2010) 024707.
[16] J. Li, A.F.T. Yokochi, A.W. Sleight, Solid State Sciences 6 (2004) 831.
[17] Y. Kakehi, K. Satoh, T. Yoshimura, A. Ashida, N. Fujimura, Vacuum 84 (2009) 618.
[18] D. Li, X.D. Fang, Z.H. Deng, W.W. Dong, R.H. Ta, S. Zhou, J.M. Wang, T. Wang, Y.P. Zha, X.B. Zhu, Journal of Alloys and Compounds 486 (2009) 462.
[19] A. Maignan, V. Eyert, C. Martin, S. Kremer, R. Fresard, D. Pelloquin, Physical Review B 80 (2009) 115103.
[20] R. Manoj, M. Nisha, K.A. Vanaja, M.K. Jayaraj, Bulletin of Materials Science 31 (2008) 49.
[21] H. Yanagi, T. Hase, S. Ibuki, K. Ueda, H. Hosono, Applied Physics Letters 78 (2001) 1583.
[22] K. Hayashi, T. Nozaki, T. Kajitani, Japanese Journal of Applied Physics Part 1 46 (2007) 5226.
[23] P.W. Sadik, M. Ivill, V. Craciun, D.P. Norton, Thin Solid Films 517 (2009) 3211.
[24] R. Nagarajan, A.D. Draeseke, A.W. Sleight, J. Tate, Journal of Applied Physics 12 (2001) 8022.
[25] A. Maignan, C. Martin, R. Fresard, V. Eyert, E. Guilmeau, S. Hebert, M. Poienar, D. Pelloquin, Solid State Communications 149 (2009) 964.
[26] G.B. Dong, M. Zhang, W. Lan, P.M. Dong, H. Yan, Vacuum 82 (2008) 1321.
[27] Y. Kumekawa, M. Hirai, Y. Kobayashi, S. Endoh, E. Oikawa, T. Hashimoto, Journal of Thermal Analysis and Calorimetry 99 (2010) 57.
[28] M.S. Lee, T.Y. Kim, D. Kim, Applied Physics Letters 79 (2001) 13.
[29] S.H. Lim, S. Desu, A.C. Rastogi, Journal of Physics and Chemistry of Solids 69 (2008) 2047.
[30] J. Tauc, A. Menth, Journal of Non-Crystalline Solids 8 (1972) 569.
[31] C.H. Ong, H. Gong, Thin Solid Films 445 (2003) 299.
[32] M.N. Huda, Y.F. Yan, A. Walsh, S.H. Wei, M.M. Al-Jassim, Physical Review B 80 (2009) 035205.
[33] D.O. Scanlon, K.G. Godinho, B.J. Morgan, G.W. Watson, Journal of Chemical Physics 132 (2010) 024707.
[34] J. Li, A.F.T. Yokochi, A.W. Sleight, Solid State Sciences 8 (2004) 831.
[35] E. Mugnier, A. Barnabe, P. Tailhades, Solid State Ionics 177 (2006) 607.
[36] G.B. Dong, M. Zhang, T.X. Li, H. Yan, Journal of the Electrochemical Society 157 (2010) H127.
[37] P.M. Dong, M. Zhang, G.B. Dong, X.P. Zhao, H. Yan, Journal of the Electrochemical Society 155 (2008) H319.
[38] J. Tate, H.L. Ju, J.C. Moon, A. Zakutayev, A.P. Richard, J. Russell, D.H. Mcintyre, Physical Review B 80 (2009) 165206.